Nanoscale

ROYAL SOCIETY OF CHEMISTRY

COMMUNICATION

View Article Online
View Journal | View Issue

Cite this: *Nanoscale*, 2024, **16**, 19221

Received 11th July 2024,
Accepted 29th September 2024

DOI: 10.1039/d4nr02872d

rsc.li/nanoscale

Simultaneous formation of helical and sheet-like assemblies from short azapeptides enables spontaneous resolution†

Xiaosheng Yan, *[a,b] Peimin Weng,[a] Jinlian Cao,[a] Kexin Lin,[b] Yuanwei Qi,[b] Xin Wu [b] and Yun-Bao Jiang *[a]

As determined by the homochirality of amino acid building units, protein secondary structures α-helix and β-sheet are single-handed chiral superstructures extending in one and quasi-two dimensions, respectively. Synthetic molecular assemblies that mimic the structural homochirality of proteins would provide insights into the origin of biological homochirality and inform the development of chiral separation techniques. Here we fabricated a homochiral 3D assembly consisting of 1D helical and 2D sheet-like assemblies that feature molecular packings resembling α-helix and β-sheet, respectively. This was achieved by using an alanine derivative, a β-turn structured short azapeptide from *p*-iodobenzoylalanine-based *N*-amido-*N*′-phenylthiourea. While N–H···S=C/O=C hydrogen bonds between the β-turn scaffolds afford a 2D pleated sheet-like structure, the head-to-tail C–I···π halogen bonds, together with the N–H···O=C hydrogen bonds, support a 1D helical-like assembly, serving as linkers to connect the 2D sheet-like structures into a 3D superstructure. The two biomimetic assembly modes share the N–H···O=C hydrogen bonds and can allow 3D homochiral elongation, driving spontaneous resolution of the short azapeptides to generate conglomerate crystals.

[a]*Department of Chemistry, College of Chemistry and Chemical Engineering, The MOE Key Laboratory of Spectrochemical Analysis and Instrumentation, and iChEM, Xiamen University, Xiamen 361005, China. E-mail: xshyan@xmu.edu.cn, ybjiang@xmu.edu.cn*

[b]*Fujian Provincial Key Laboratory of Innovative Drug Target Research and State Key Laboratory of Cellular Stress Biology, School of Pharmaceutical Sciences, Xiamen University, Xiamen, Fujian 361102, China*

†Electronic supplementary information (ESI) available: The crystal data and other experimental data. CCDC 1998159, 1998160, 1998162, 1998163 and 2068984. For ESI and crystallographic data in CIF or other electronic format see DOI: https://doi.org/10.1039/d4nr02872d

Xiaosheng Yan

Xiaosheng Yan obtained his Bachelor's degree in applied chemistry from Huazhong Agricultural University in 2010, and his PhD degree in analytical chemistry from Xiamen University in 2016 under the supervision of Professor Yun-Bao Jiang. From 2016 to 2021, he worked as a postdoctoral researcher and then a research assistant at Xiamen University. He joined the School of Pharmaceutical Sciences of Xiamen University as an associate professor in 2021. His research interests are centered on peptidomimetics for biomimetic recognition, assembly, transport and anticancer therapy.

Introduction

Understanding the origin of biological homochirality is a long-standing challenge.[1–3] Conglomerate crystallization is a spontaneous resolution phenomenon, *i.e.* the fact that different enantiomers reside in separate crystals, which provides a hypothesis to the origin of biological homochirality, and also allows the production of enantiopure compounds.[4,5] While this was first discovered in 1848 by Louis Pasteur's tartrate salt crystallization experiments,[6] rational design of molecules that undergo conglomerate crystallization remains challenging.[7,8] Conglomerate behavior means that the enantiopure crystals (homochiral 3D structures) are favored over the alternative racemic crystals (heterochiral 3D structures).[8] In this context, biological α-helix and β-sheet, the two major secondary structures that are central to the structures and functions of natural peptides/proteins consisting of homochiral L-amino acid residues,[9,10] can be regarded as 1D and quasi-2D homochiral structures, respectively. We thus hypothesized that the combination of homochiral α-helix and β-sheet mimics, *e.g.* 1D helical and 2D sheet-like assemblies, would result in a 3D homochiral structure (Scheme 1a), potenially leading to conglomerare crystals that feature spontaneous resolution.

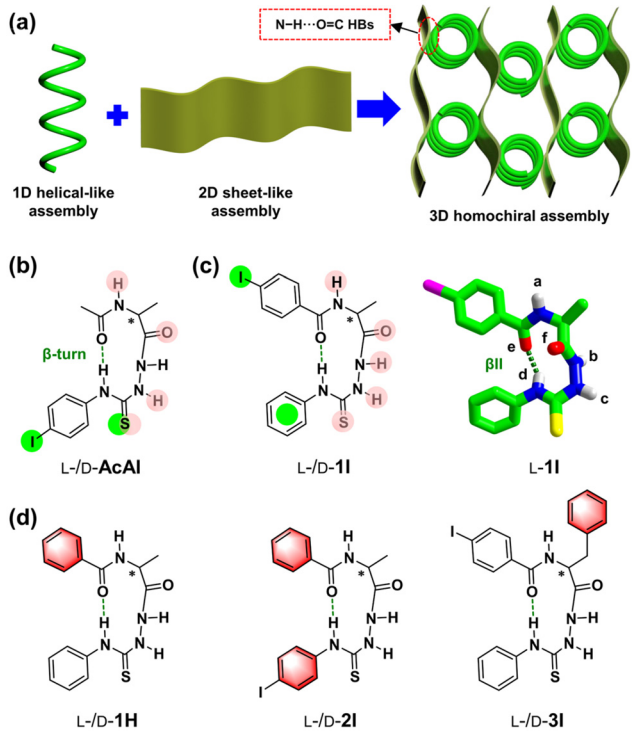

Scheme 1 (a) Schematic representation of the 3D homochiral assembly consisting of 1D helical and 2D sheet-like assemblies, wherein amide-amide type hydrogen bonds (N–H···O=C HBs) are shared in the two biomimetic assemblies. (b) Chemical structure of **AcAI** with a β-turn structure in previous work.[35] The green balls indicate halogen bonding sites, light red balls highlight hydrogen bonding sites. (c) Chemical structure of *p*-iodobenzoylalanine based *N*-amido-*N*′-phenylthiourea **1I** and crystal structure of L-**1I** with a βII-turn. The green balls indicate potential sites of intermolecular halogen bonding, light red balls highlight potential sites of intermolecular hydrogen bonding. For clarity, –CH protons in the crystal structure are omitted. (d) Chemical structures of control compounds **1H**, **2I** and **3I**. Intramolecular hydrogen bonds for β-turn structure are highlighted by green dashed lines.

The amide-amide type (N–H···O=C) hydrogen bonds are responsible for maintaining both α-helix and β-sheet structures.[9,10] By sharing these hydrogen bonds, one could potentially combine 1D helical and 2D sheet-like assemblies into a homochiral 3D assembly, wherein 1D helices serve as linkers to connect homochiral 2D sheet-like planes (Scheme 1a). In the helical-like assemblies, the hydrogen bonds or other functionally equivalent interactions primarily form between homochiral components, leading to a 1D homochiral structure.[11–13] However, in the β-sheet organization, the hydrogen bonds can occur between either homochiral or heterochiral building blocks, resulting in homochiral 2D pleated planes or racemic 2D rippled planes,[10,14–17] representing a key challenge for exploiting sheet-like structures for spontaneous resolution purposes. We envision that by sharing the hydrogen bonds in helical and sheet-like assemblies, the formation of racemic rippled sheets can be prevented while facilitating the formation of homochiral pleated sheets. Ultimately, this would enable the generation of a 3D homochiral structure.

We have thus decided to develop a small-molecule based 3D supramolecular structure consisting of helical and sheet-like assemblies. The immediate inspiration is to use a short peptide as the building block. While short peptides primarily assemble into β-sheet-like structures *via* amide-amide hydrogen bonding,[18–21] making short peptides into a helical structure is a feasible pathway to helical-like assembly, in case that suitable head-to-tail intermolecular interactions are explored to allow a well-propagation of the helicity of helical short peptides.[22–26]

We showed that derivatizing the *C*-terminus of a short peptide into *N*-amidothiourea leads to a rich family of helical short azapeptides containing a β-turn structure (exampled in Scheme 1b),[27–29] which function as helical building blocks to form supramolecular helices *via* intermolecular halogen and chalcogen bonds.[30–34] Very importantly, we recently showed that folded short azapeptide of acetylalanine-based *N*-amido-*N*′-phenylthiourea containing a *C*-terminal iodine substituent (**AcAI**, Scheme 1b) can form orthogonal hydrogen- and halogen-bonded homochiral helices in two dimensions. In this case, the hydrogen bonding domain is situated in the central peptide backbone, while the halogen bonding domain is positioned at the *C*-terminus, involving only a partial β-turn scaffold in the two helical chains. The resultant two helices facilitate 3D homochiral elongation and consequently promote spontaneous resolution.[35]

Here we proposed to relocate the *C*-terminal iodine substituent to the *N*-terminus, resulting in *p*-iodobenzoylalanine based *N*-amido-*N*′-phenylthiourea (**1I**, Scheme 1c). This adjustment positions the halogen bonding domain at the two termini, *i.e.* iodophenyl and phenyl groups, enabling head-to-tail C–I···π halogen bonds to accommodate the entire β-turn structure in a 1D helical-like organization. Simultaneously, the vacant amide-amide type hydrogen bonds formed by –NH and –C=O/S groups in the peptide backbone could support a 2D sheet-like assembly, akin to the β-sheet organization from general short peptides, potentially stabilizing the halogen-bonded helical-like organization as well. Alanine residue is used since it is a decent amino acid residue involved in both α-helix and β-sheet,[36] and the small steric hindrance of its side chain could accommodate the occurrence of both structures. Indeed, we successfully created a 3D superstructure consisting of 1D helical and 2D sheet-like assemblies in the crystals of **1I**, underpinned by amide-amide hydrogen bonding and C–I···π halogen bonding, with a 3D-homochirality and therefore spontaneous resolution to generate conglomerate crystals from racemic **1I** (*rac*-**1I**).

Results and discussion

Crystal structures of 1I

Short peptide-based *N*-amidothioureas **1I**, **1H**, **2I** and **3I** were synthesized following the procedures shown in Schemes S1–S3.† The crystals of L-**1I** was readily obtained from its iPrOH solution upon slow solvent evaporation (for detailed crystallo-

graphic data, see Table S1†), exhibiting a folded βII-turn structure (Scheme 1c), maintained by ten-membered ring intramolecular hydrogen bond (N–H^{d}···^{e}O=C, structural parameters of β-turns given in Table S2†).

Molecular packing in L-**1I** crystals is next examined. Along the crystallographic *b*-axis, L-**1I** molecules are linked *via* head-to-tail N–H^{a}···S=C hydrogen bonds (Fig. S1a and Table S3†), resulting in a strand-like 1D array resembles a β-strand structure (Fig. 1a). The torsion of two consecutive H^{a}···S hydrogen bonds (H^{a}SH^{a}S) is −13.05°, indicating that the 1D strand-like assembly is slightly twisted, similar to biological β-strands that almost all have a twist of 13° (Table 1).[37,38]

Along *a*-axis, parallel strand-like assemblies of L-**1I** are linked by N–H^{a}···^{f}O=C hydrogen bonds (Fig. S1b†), affording a 2D pleated sheet-like assembly within *ab* plane (Fig. S1c†), which resembles a parallel β-sheet structure in proteins (Fig. 1b and Table 1).[10] While the N–H^{a}···S=C hydrogen bonds play the role of intra-strand amide bonds in a β-strand to lead to a 1D structure, the N–H^{b}···^{f}O=C hydrogen bonds function as the typical inter-strand N–H···O=C hydrogen bonds in protein β-sheet to lead to a pleated 2D superstructure of L-**1I** (Fig. 1b). The iodophenyl and phenyl rings are oriented alternatively at the two sides of the pleated sheet (Fig. S1c† and Fig. 2a), resembling the side chains of amino acid residues in biological β-sheet.[10]

Along crystallographic *c*-axis, iodophenyl and phenyl rings between adjacent sheet-like assemblies of L-**1I** form intermolecular C–I···π interactions (3.896 Å in distance and 163.67° in angle, Table S3 and Fig. S2†),[30,39] linking those 2D pleated structures into a 3D assembly (Fig. 2a). Natural bond orbital (NBO) analysis[40] demonstrates the electronic acceptor nature of σ*(I–C) orbital (Table S4†), indicating the occurrence of C–I···π halogen bonding. This observation is further supported by the topology paths analyzed using the quantum theory of atoms in molecules (QTAIM),[41] showing a strength of *ca.* −6.76 kJ mol^{-1} for the local C–I···π halogen bonding in the L-**1I** dimer (Table S5†). Additionally, the noncovalent interaction (NCI) analysis suggests a weakly attractive interaction (Fig. S3†).[42]

Table 1 Comparison between classical protein parallel β-sheet and sheet-like assembly of L-**1I**

Structural attribute	Protein parallel β-sheet	Sheet of L-**1I**
Building blocks	L-Amino acids	L-**1I** molecules
Twist angle of a strand	13° [a]	−13.05°
Adjacent strands	Parallel	Parallel
Supporting interactions	Amide bonds	N–H^{a}···S=C HBs
	N–H···O=C HBs	N–H^{b}···^{f}O=C HBs

[a] The most frequent value of twist angle of a strand.[37,38]

The C–I···π halogen bonds extend in a helical fashion that well propagate the helicity of the β-turn structure along *a*-axis, resulting in a supramolecular right-handed *P*-helix with a pitch of 4.66 Å (Fig. 2b). This helical-like assembly is further stabilized by N–H^{b}···^{f}O=C hydrogen bonds, which also support the sheet-like 2D assembly (Fig. 1b). The formed *P*-helix from L-**1I** is reminiscent of the classical protein α-helix (Table 2).[9] The C–I···π halogen bonds function like amide bonds to link the short peptides in a head-to-tail helical fashion, while the N–H^{b}···^{f}O=C hydrogen bonds stabilize the helical conformation analogously to those found in the protein α-helix.

Iodine, when connected to a common benzene ring without any electron-withdrawing groups, lacks significant electron deficiency to act as a donor for halogen bonding.[39] However, in the crystal of L-**1I**, the propagation of β-turn helicity,[30] together with the N–H^{b}···^{f}O=C hydrogen bonds, facilitates the formation of C–I···π halogen bonds. This cooperative effect ultimately contributes to the formation of helical-like assembly of L-**1I**. Notably, the hydrogen- and halogen-bonded *P*-helix from L-**1I** along *a*-axis is different from our previously devel-

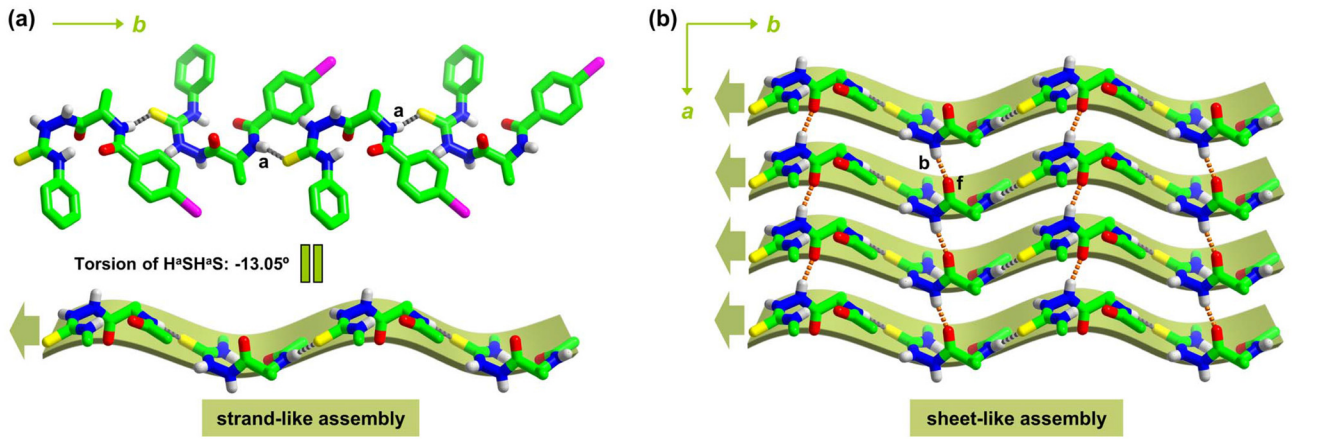

Fig. 1 (a) Strand-like 1D assembly along *b*-axis from L-**1I** molecules *via* intermolecular N–H^{a}···S=C hydrogen bonds (dashed gray lines). (b) N–H^{b}···^{f}O=C hydrogen bonds (dashed orange lines) along *a*-axis link parallel strand-like 1D assemblies into a sheet-like 2D assembly within *ab* plane. For clarity, –CH protons are omitted, in the strand and sheet-like assemblies, iodophenyl and phenyl rings are also omitted. The thick arrows indicate the direction of *N*- to *C*-terminus of L-**1I** along the strand structure.

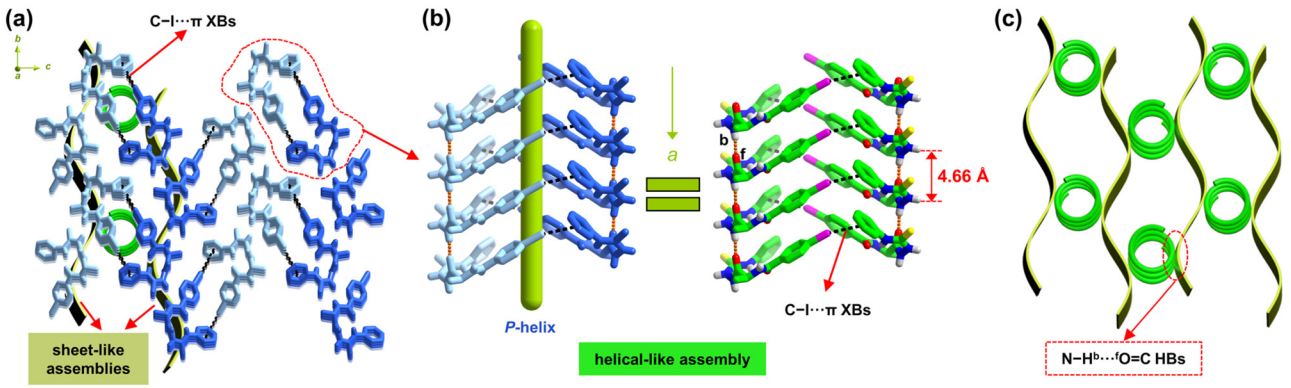

Fig. 2 (a) 3D superstructure identified in L-**1I** crystal, in which the C–I···π halogen bonds (XBs, dashed black lines) along *c*-axis link the sheet-like 2D assemblies into a 3D structure. (b) Supramolecular *P*-helix of L-**1I** molecules along *a*-axis maintained by helical C–I···π halogen bonds (XBs, dashed black lines) and further stabilized by N–H^{b}···^{f}O=C hydrogen bonds (dashed orange lines), reminiscent of classical α-helix. For clarity, –CH protons are omitted. (c) Schematic representation of 3D assembly of L-**1I** crystal consisting of 1D helical and 2D sheet-like assemblies, wherein N–H^{b}···^{f}O=C hydrogen bonds are shared in the two biomimetic assemblies.

Table 2 Comparison between classical protein α-helix and supramolecular helix of L-**1I**

Structural attribute	Protein α-helix	Helix from L-**1I**
Building blocks	L-Amino acids	L-**1I** molecules
Helical sense	Right-handed (*P*-)	Right-handed (*P*-)
One helical pitch	3.6 residues	2 L-**1I** molecules
Pitch length	5.4 Å	4.66 Å
Supporting interactions	Amide bonds	C–I···π XBs
	N–H···O=C HBs	N–H^{b}···^{f}O=C HBs

oped orthogonal helices in two dimensions from **AcAI** (Scheme 1b), which consist of one hydrogen-bonded helix and one halogen-bonded helix along two different crystallographic axes.[35]

Therefore, in the crystals L-**1I** molecules simultaneously form sheet-like 2D pleated assembly (Fig. 1b) and helical-like 1D assembly (Fig. 2b), resembling biological β-sheet and α-helix, respectively. The former is maintained by N–H^{a}···S=C and N–H^{b}···^{f}O=C hydrogen bonds, and the latter by C–I···π halogen bonds and N–H^{b}···^{f}O=C hydrogen bonds. The shared N–H^{b}···^{f}O=C hydrogen bonds link the two biomimetic assemblies into a 3D homochiral assembly (Fig. 2c).

Crystals of D-**1I** from iPrOH solution were also obtained, showing a βII′-turn structure (Fig. S4 and Table S2†). A 3D-superstructure consisting of 2D sheet and 1D helical-like (*M*-helix) assemblies has also been identified in D-**1I** crystal (Fig. S5 and S6†), which is mirror symmetric to that of L-**1I** crystal.

Spontaneous resolution of 1I

It was envisaged that the combination of helical and sheet-like assemblies in enantiopure **1I** crystals would drive 3D homochirality, and thereby promote spontaneous resolution upon crystallization. We thus grew *rac*-**1I** crystals from iPrOH. Indeed, the determined space group of *rac*-**1I** crystals is Sohncke $P2_12_12_1$, and the crystals are identified to be either of enantiopure L-**1I** or enantiopure D-**1I** by X-ray crystallographic analysis (Table S6†), suggesting that the racemate undergoes a spontaneous resolution and forms conglomerate. This is further supported by identical X-ray powder diffraction (XRPD) patterns of L-**1I** and *rac*-**1I** (Fig. 3), and high-performance liquid chromatography (HPLC) traces of the selected single crystals (ee > ±97%, Fig. S7†).

The propagation of the β-turn helicity of **1I** could promote homochiral elongation along the twisted strand-like assembly supported by N–H^{a}···S=C hydrogen bonds (Fig. 1a). Additionally, the formation of 1D helical-like assembly would help propagate the helicity of β-turn structure, facilitating homochiral elongation along C–I···π halogen bonding and N–H^{b}···^{f}O=C hydrogen bonding (Fig. 2b). The latter interaction drives homochiral stacking of 1D strand-like assemblies along *a*-axis to generate a homochiral 2D sheet-like assembly (Fig. 1b), preventing the formation of racemic rippled sheet-like structures.[14–17] Hence, 3D homochirality occurs in **1I** crys-

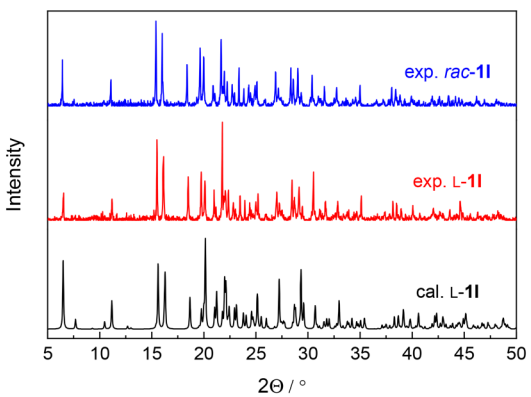

Fig. 3 Calculated and experimental XRPD patterns of L-**1I** crystals and experimental XRPD of *rac*-**1I** crystals grown in iPrOH. The identical XRPDs of L-**1I** and *rac*-**1I** crystals indicate that *rac*-**1I** forms racemic conglomerates.

tals, wherein the sharing of N–H^{b}···^{f}O=C hydrogen bonds in both the biomimetic helical and sheet-like assemblies play a role.

Scanning electron microscopy (SEM) images on platinum-coated silicon wafers of air-dried samples of L-**1I** reveal fiber-like structures at a low concentration of 10 μM in iPrOH, which transition to well-ordered rods at a higher concentration of 1 mM (Fig. S8†). The former can be attributed to helical-like assemblies, whereas the latter are formed from a combination of helical and sheet-like assemblies, which is consistent with the crystal structures. Similarly, *rac*-**1I** exhibits concentration-dependent SEM images (Fig. S8†), supporting its property of spontaneous resolution.

Crystal structures of 1H

To illustrate the role of C–I···π halogen bonding in maintaining the helical-like assembly and in promoting 3D homochirality for spontaneous resolution, **1H** without iodine substituent was designed and investigated (Scheme 1d). Enantiopure L-**1H** and D-**1H** crystals were readily obtained from iPrOH *via* slow evaporation (Table S7†). In crystals, L-**1H** shows a folded βII-turn structure (Fig. S9†) and forms a sheet-like 2D assembly within *ab* plane, *via* N–H^{a}···S=C hydrogen bonds along *b*-axis and N–H^{b}···^{f}O=C hydrogen bonds along *a*-axis (Fig. S10†), similar to that in L-**1I** crystal (Fig. 1).

Along *c*-axis, 2D sheet-like assemblies from L-**1H** molecules stack *via* van der Waals interactions to lead to a 3D superstructure (Fig. 4a). Due to the polar nature of L-**1H** characterized by a dipole moment of 9.33 D (Fig. S11†), the dipole–dipole interactions are suggested to make a substantial contribution to the overall van der Waals interactions. Interestingly, N–H^{b}···^{f}O=C hydrogen bonding and van der Waals interactions between L-**1H** molecules result in a supramolecular quasi-*P*-helix (quasi-α-helix mimic) along *a*-axis (4.71 Å pitch, Fig. 4b). The term "quasi-" refers to the fact that the van der Waals interactions (Fig. 4b) that maintain the helix are non-directional and weak. Therefore, the 3D superstructure of L-**1H** crystal can be regarded as the combination of 1D quasi-helical and 2D sheet-like assemblies *via* the sharing of N–H^{b}···^{f}O=C hydrogen bonds. The 3D superstructure of the D-**1H** crystal is mirror symmetric to that of L-**1H** crystal (Fig. S9, S12 and S13†).

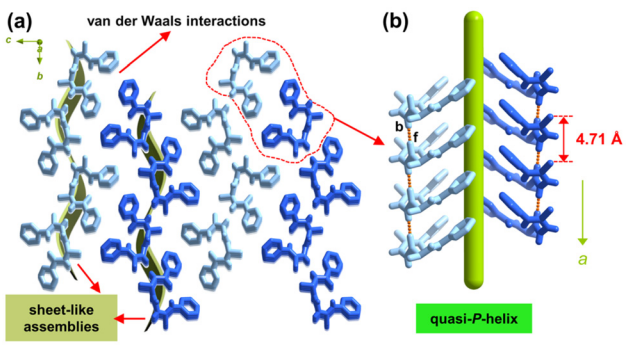

Fig. 4 (a) 3D superstructure of L-**1H** crystal, in which sheet-like 2D structures stack *via* van der Waals interactions along *c*-axis to form a 3D structure. (b) Supramolecular quasi-*P*-helix from L-**1H** molecules along *a*-axis supported by N–H^{b}···^{f}O=C hydrogen bonds (dashed orange lines) and van der Waals interactions. For clarity, –CH protons are omitted.

Structural comparison of 1I and 1H

The geometrical parameters and interaction energies analysed by QTAIM of the intramolecular hydrogen bonds indicate that β-turn of L-**1I** is more favorable than that of L-**1H** (2.117 Å *vs.* 2.392 Å in distance of H^{d}···O^{e}, 149.40° *vs.* 137.94° in angle of NH^{d}O^{e}, −11.8 kJ mol^{-1} *vs.* −5.76 kJ mol^{-1} in interaction energy, Table S2†). However, in the solution phase where the azapeptides exist in the monomeric form,[27–29] the strength of β-turn structure in L-**1I** and L-**1H** is comparable, demonstrated by almost the same solvent accessibility of the thioureido –NH^{d} protons that are involved in the intramolecular hydrogen bonding (Fig. S14†). It is therefore not the intramolecular electronic effect of the iodine substituent, but rather the intermolecular interactions driven superstructures are responsible for the more stable β-turn structure of L-**1I** than that of L-**1H** in the crystal state.

According to crystal structures, we note that the packing mode in the L-**1H** crystal (Fig. S10† and Fig. 4) is similar with that in the L-**1I** crystal (Fig. 1 and 2), consistent with their comparable profiles of Fourier transform infrared (FTIR) spectra (Fig. 5a), wherein the amide I bands at 1681/1682 cm^{-1} can be attributed to C=O^{e} groups that form β-turns, while the bands at 1647/1650 cm^{-1} correspond to C=O^{f} groups that participate in both helical/quasi-helical and sheet-like assemblies.[43] The absorption and CD spectra of L-**1I** and L-**1H** crystals were measured (Fig. S15†), through which their *g* factor profiles were obtained. The two crystals show similar spectral profiles, but the maximum *g* factor of L-**1I** crystal is higher than that of L-**1H** crystal (1.3×10^{-3} *vs.* 0.78×10^{-3}, Fig. 5b).[44] This indicates the stronger optical activity of L-**1I** crystal than that of L-**1H** crystal. Note that directional and strong C–I···π halogen bonding in L-**1I** crystals is absent in L-**1H** crystals, where non-directional and weak van der Waals interactions are employed to stabilize the 3D superstructure in L-**1H** crystal. This could

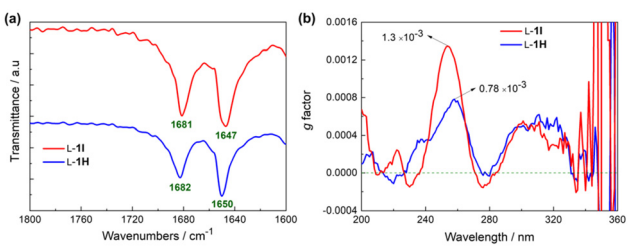

Fig. 5 (a) FTIR spectra of L-**1I** and L-**1H** crystals. (b) The *g* factor profiles of L-**1I** and L-**1H** crystals. Note that the positive signals at long wavelengths (280–320 nm) agree with the *P*-helicity observed in the crystal structures.

lead to weaker supramolecular helicity and stability of L-**1H** crystal, accounting for the less favorable β-turn and lower maximum *g* factor of L-**1H** crystal than those of L-**1I** crystal (Table S2† and Fig. 5b), as well as the depressed spontaneous resolution property of **1H** (*vide infra*).

Spontaneous resolution property of 1H

For *rac*-**1H** crystals grown in iPrOH, the space group is Sohncke $P2_12_12_1$ (Table S8†), and the XRPD patterns of L-**1H** and *rac*-**1H** are identical (Fig. S16†), indicative of conglomerate formation from *rac*-**1H**. However, the Flack parameters of determined crystals are much greater than 0 (from −0.48 to 0.35, Table S8†). Moreover, the chiral HPLC measurements show that the ee of selected *rac*-**1H** crystals vary between −58% and 9.2% (Table S9†). This can be explained by the formation of epitaxial racemic conglomerates from *rac*-**1H** in iPrOH, generating laminar crystals composed of alternating homochiral layers from the opposite enantiomers (Fig. S17†).[45,46]

While the epitaxial racemic conglomerate formation arises from the interplay between mass transport and surface kinetics,[45] the phenomenon also indicates that the capacity of 3D homochiral elongation of **1H** is not so sufficiently strong to suppress such undesired interplay. We also grew *rac*-**1H** crystals in CH_3OH solution, which are in $P2_1/n$ space group (Table S7†). This confirms the co-crystallization of L-**1H** and D-**1H** into a racemic compound, further indicated by the crystal structures (Fig. S18–S21†). The XRPD patterns of L-**1H** and *rac*-**1H** crystals grown in CH_3OH are different (Fig. S22†), while chiral HPLC trace of one single *rac*-**1H** crystal shows equal amounts of L-**1H** and D-**1H** (Fig. S23†).

Our previous work[35] and the classic example of racemic DNA crystals[47] indicate that a single 1D helical-like assembly is insufficient to achieve 3D homochirality in conglomerate crystallization. Upon analysing the crystal structures and spontaneous resolution property of **1I** and **1H**, it becomes clear that relying solely on the sheet-like assembly is also inadequate for conglomerate crystallization. Both the stable helical and sheet-like assemblies are required for the spontaneous resolution of **1I** to occur to generate conglomerate crystals.

Control compounds 2I and 3I

Similar hydrogen bonding modes observed in **1H** and **1I** crystals suggest that hydrogen and halogen bonding in **1I** are orthogonal. We thus decided to move iodine substituent to the *C*-terminal phenyl ring, generating control compound **2I** (Scheme 1d). We, however, were unable to grow the crystals of enantiopure and racemic **2I** in iPrOH, CH_3OH and many other solvents, suggesting that the hydrogen and halogen bonding in **1I** have indeed facilitated its crystallization to form homochiral 3D structure. Crystallization of **3I** (Scheme 1d), the phenylalanine derivative of **1I**, was also unsuccessful, possibly due to the large steric hindrance of the phenyl substituent in phenylalanine residue that prevents the simultaneous occurrence of helical and sheet-like assemblies that may mixed into a well-ordered homochiral 3D structure.

Conclusions

In summary, we have demonstrated that the combination of biomimetic 1D helical and 2D sheet-like assemblies can generate a homochiral 3D assembly to facilitate the spontaneous resolution. The short azapeptide containing a helical β-turn structure, *p*-iodobenzoylalanine-based *N*-amido-*N*′-phenylthiourea, was designed as a proof-of-concept, wherein amide-amide type N–H···S═C/O═C hydrogen bonds between the peptide backbones support a 2D pleated sheet-like assembly that is reminiscent of biological parallel β-sheet. Furthermore, the terminal iodophenyl and phenyl groups afford the head-to-tail C–I···π halogen bonds to hold the entire β-turn structure into a 1D helical-like assembly that resembles α-helix, which is further stabilized by the N–H···O═C hydrogen bonds that have also occurred in the sheet-like assembly. The shared N–H···O═C hydrogen bonds allows the combination of helical and sheet-like assemblies to produce a 3D chiral architecture, featuring 3D homochiral elongation and eventually promoting spontaneous resolution of the short azapeptides. Our results suggest that biomimetic high-order chiral structures, *e.g.* α-helix and β-sheet mimics, could lead to chiral self-sorting, which could promote the understanding of biological homochirality. Our studies also provide guidance for designing molecules that undergo spontaneous chiral resolution.

Data availability

Crystallographic data for L-**1I**, D-**1I**, L-**1H**, D-**1H** and *rac*-**1H** have been deposited at the CCDC under 1998159, 1998160, 1998162, 1998163 and 2068984.†

Conflicts of interest

There are no conflicts to declare.

Acknowledgements

We thank the support of this work by the Natural Science Foundation of China (Grants 21820102006, 22101240, 22241503 and 92356308), the Fundamental Research Funds for the Central Universities (Grants 20720220005 and 20720220121), the Natural Science Foundation of Fujian Province of China (No. 2023J01038) and Nanqiang Youth Scholar Program of Xiamen University.

References

1 K. Ruiz-Mirazo, C. Briones and A. de la Escosura, *Chem. Rev.*, 2014, **114**, 285–366.
2 A. Brewer and A. P. Davis, *Nat. Chem.*, 2014, **6**, 569–574.

3 M. Deng, J. Yu and D. G. Blackmond, *Nature*, 2024, **626**, 1019–1024.
4 J. I. Putman and D. W. Armstrong, *Chirality*, 2022, **34**, 1338–1354.
5 J. Sui, N. Wang, J. Wang, X. Huang, T. Wang, L. Zhou and H. Hao, *Chem. Sci.*, 2023, **14**, 11955–12003.
6 L. Pasteur, *Ann. Chim. Phys.*, 1848, **24**, 442–459.
7 M. P. Walsh, J. A. Barclay, C. S. Begg, J. Xuan and M. O. Kitching, *Cryst. Growth Des.*, 2023, **23**, 2837–2844.
8 P. Weng, X. Yan and Y.-B. Jiang, *ChemSystemsChem*, 2023, **5**, e202200043.
9 L. Pauling, R. B. Corey and H. R. Branson, *Proc. Natl. Acad. Sci. U. S. A.*, 1951, **37**, 205–211.
10 L. Pauling and R. B. Corey, *Proc. Natl. Acad. Sci. U. S. A.*, 1951, **37**, 251–256.
11 M. Liu, L. Zhang and T. Wang, *Chem. Rev.*, 2015, **115**, 7304–7397.
12 E. Yashima, N. Ousaka, D. Taura, K. Shimomura, T. Ikai and K. Maeda, *Chem. Rev.*, 2016, **116**, 13752–13990.
13 H. Jędrzejewska and A. Szumna, *Chem. Rev.*, 2017, **117**, 4863–4899.
14 I. Weissbuch, R. A. Illos, G. Bolbach and M. Lahav, *Acc. Chem. Res.*, 2009, **42**, 1128–1140.
15 R. J. Swanekamp, J. T. M. DiMaio, C. J. Bowerman and B. L. Nilsson, *J. Am. Chem. Soc.*, 2012, **134**, 5556–5559.
16 J. A. Raskatov, J. P. Schneider and B. L. Nilsson, *Acc. Chem. Res.*, 2021, **54**, 2488–2501.
17 A. J. Kuhn, B. Ehlke, T. C. Johnstone, S. R. J. Oliver and J. A. Raskatov, *Chem. Sci.*, 2022, **13**, 671–680.
18 P. W. J. M. Frederix, G. G. Scott, Y. M. Abul-Haija, D. Kalafatovic, C. G. Pappas, N. Javid, N. T. Hunt, R. V. Ulijn and T. Tuttle, *Nat. Chem.*, 2015, **7**, 30–37.
19 S. Bera, S. Mondal, S. Rencus-Lazar and E. Gazit, *Acc. Chem. Res.*, 2018, **51**, 2187–2197.
20 P. Chakraborty, S. Bera, P. Mickel, A. Paul, L. J. W. Shimon, Z. A. Arnon, D. Segal, P. Král and E. Gazit, *Angew. Chem., Int. Ed.*, 2022, **61**, e202113845.
21 J. Cao, P. Weng, Y. Qi, K. Lin and X. Yan, *Chem. Commun.*, 2024, **60**, 1484–1487.
22 S. Mondal, L. Adler-Abramovich, A. Lampel, Y. Bram, S. Lipstman and E. Gazit, *Nat. Commun.*, 2015, **6**, 8615.
23 R. Misra, A. Saseendran, S. Dey and H. N. Gopi, *Angew. Chem., Int. Ed.*, 2019, **58**, 2251–2255.
24 S. Dey, R. Misra, A. Saseendran, S. Pahan and H. N. Gopi, *Angew. Chem., Int. Ed.*, 2021, **60**, 9863–9868.
25 T. Sawada and M. Fujita, *Chem*, 2020, **6**, 1861–1876.
26 X. Yan, P. Weng, D. Shi and Y.-B. Jiang, *Chem. Commun.*, 2021, **57**, 12562–12574.
27 X.-S. Yan, K. Wu, Y. Yuan, Y. Zhan, J.-H. Wang, Z. Li and Y.-B. Jiang, *Chem. Commun.*, 2013, **49**, 8943–8945.
28 X.-S. Yan, H. Luo, K.-S. Zou, J.-L. Cao, Z. Li and Y.-B. Jiang, *ACS Omega*, 2018, **3**, 4786–4790.
29 Y. Zhang, X. Yan, J. Cao, P. Weng, D. Miao, Z. Li and Y.-B. Jiang, *J. Org. Chem.*, 2020, **85**, 9844–9849.
30 J. Cao, X. Yan, W. He, X. Li, Z. Li, Y. Mo, M. Liu and Y.-B. Jiang, *J. Am. Chem. Soc.*, 2017, **139**, 6605–6610.
31 X. Yan, K. Zou, J. Cao, X. Li, Z. Zhao, Z. Li, A. Wu, W. Liang, Y. Mo and Y. Jiang, *Nat. Commun.*, 2019, **10**, 3610.
32 D. Shi, J. Cao, P. Weng, X. Yan, Z. Li and Y.-B. Jiang, *Org. Biomol. Chem.*, 2021, **19**, 6397–6401.
33 X. Yan, J. Cao, Y. Zhang, P. Weng, D. Miao, Z. Zhao, Z. Li and Y.-B. Jiang, *Chem. Commun.*, 2021, **57**, 1802–1805.
34 P. Weng, X. Yan, J. Cao, Z. Li and Y.-B. Jiang, *Chem. Commun.*, 2022, **58**, 6461–6464.
35 X. Lin, B. Kou, J. Cao, P. Weng, X. Yan, Z. Li and Y.-B. Jiang, *Angew. Chem., Int. Ed.*, 2022, **61**, e202205914.
36 P. Y. Chou and G. D. Fasman, *Biochemistry*, 1974, **13**, 211–222.
37 K. Fujiwara, S. Ebisawa, Y. Watanabe, H. Toda and M. Ikeguchi, *Proteins*, 2014, **82**, 1484–1493.
38 K. Fujiwara, S. Ebisawa, Y. Watanabe, H. Fujiwara and M. Ikeguchi, *BMC Struct. Biol.*, 2015, **15**, 21.
39 G. Cavallo, P. Metrangolo, R. Milani, T. Pilati, A. Priimagi, G. Resnati and G. Terraneo, *Chem. Rev.*, 2016, **116**, 2478–2601.
40 A. E. Reed, L. A. Curtiss and F. Weinhold, *Chem. Rev.*, 1988, **88**, 899–926.
41 R. F. W. Bader, *Chem. Rev.*, 1991, **91**, 893–928.
42 A. Otero-de-la-Roza, E. R. Johnson and J. Contreras-García, *Phys. Chem. Chem. Phys.*, 2012, **14**, 12165–12172.
43 V. Cabiaux, R. Brasseur, R. Wattiez, P. Falmagne, J. M. Ruysschaert and E. Goormaghtigh, *J. Biol. Chem.*, 1989, **264**, 4928–4938.
44 J. L. Greenfield, J. Wade, J. R. Brandt, X. Shi, T. J. Penfold and M. J. Fuchter, *Chem. Sci.*, 2021, **12**, 8589–8602.
45 W. J. P. van Enckevort, *J. Phys. Chem. C*, 2010, **114**, 21593–21604.
46 L. Spix, A. Alfring, H. Meekes, W. J. P. van Enckevort and E. Vlieg, *Cryst. Growth Des.*, 2014, **14**, 1744–1748.
47 P. K. Mandal, G. W. Collie, B. Kauffmann and I. Huc, *Angew. Chem., Int. Ed.*, 2014, **53**, 14424–14427.